

Article

Nanoscale Bending Dynamics in Mixed-Chain Lipid Membranes

Elizabeth G. Kelley ^{1,*} , Moritz P. K. Frewein ^{2,3} , Orsolya Czakkel ³  and Michihiro Nagao ^{1,4,5,*} ¹ Center for Neutron Research, National Institute of Standards and Technology, Gaithersburg, MD 20899, USA² Institute of Molecular Biosciences, University of Graz, NAWI Graz, 8010 Graz, Austria³ Institut Laue-Langevin, 38042 Grenoble, France⁴ Department of Materials Science and Engineering, University of Maryland, College Park, MD 20742, USA⁵ Department of Physics and Astronomy, University of Delaware, Newark, DE 19716, USA

* Correspondence: egk@nist.gov (E.G.K.); mnagao@umd.edu (M.N.)

Abstract: Lipids that have two tails of different lengths are found throughout biomembranes in nature, yet the effects of this asymmetry on the membrane properties are not well understood, especially when it comes to the membrane dynamics. Here we study the nanoscale bending fluctuations in model mixed-chain 14:0–18:0 PC (MSPC) and 18:0–14:0 PC (SMPC) lipid bilayers using neutron spin echo (NSE) spectroscopy. We find that despite the partial interdigitation that is known to persist in the fluid phase of these membranes, the collective fluctuations are enhanced on timescales of tens of nanoseconds, and the chain-asymmetric lipid bilayers are softer than an analogous chain-symmetric lipid bilayer with the same average number of carbons in the acyl tails, di-16:0 PC (DPPC). Quantitative comparison of the NSE results suggests that the enhanced bending fluctuations at the nanosecond timescales are consistent with experimental and computational studies that showed the compressibility moduli of chain-asymmetric lipid membranes are 20% to 40% lower than chain-symmetric lipid membranes. These studies add to growing evidence that the partial interdigitation in mixed-chain lipid membranes is highly dynamic in the fluid phase and impacts membrane dynamic processes from the molecular to mesoscopic length scales without significantly changing the bilayer thickness or area per lipid.

Keywords: chain-asymmetric lipids; mixed-chain lipids; collective dynamics; bending fluctuations; neutron spin echo (NSE)



Citation: Kelley, E.G.; Frewein, M.P.K.; Czakkel, O.; Nagao, M.

Nanoscale Bending Dynamics in Mixed-Chain Lipid Membranes. *Symmetry* **2023**, *15*, 191. <https://doi.org/10.3390/sym15010191>

Academic Editor: Haruo Hosoya

Received: 2 December 2022

Revised: 19 December 2022

Accepted: 29 December 2022

Published: 9 January 2023



Copyright: © 2023 by the authors. Licensee MDPI, Basel, Switzerland. This article is an open access article distributed under the terms and conditions of the Creative Commons Attribution (CC BY) license (<https://creativecommons.org/licenses/by/4.0/>).

1. Introduction

Subtle changes in the chemical structure of lipid molecules are known to significantly affect the physical properties of biomembranes. Systematic studies of model systems have revealed that changes in the number of carbons and degree of unsaturation in the lipid acyl tails directly impact the properties of the resulting model membranes. For example, at a given temperature, the bilayer thickness (d_B), bending modulus (κ) and membrane viscosity all increase as the number of carbons in saturated lipid tails increases [1–6]. Meanwhile, introducing a single degree of unsaturation reduces the melting temperature (T_m) and disorders the tail packing while increasing the area per lipid (A_L) compared to a membrane composed of a saturated lipid with the same number of carbons in the acyl tail [7].

While most lipids have two tails that are similar in chain length [8], an unusual and historically less studied class of lipid molecules are those with mixed acyl tails that differ in chain length by several carbons, often referred to as ‘tail-asymmetric’ or ‘mixed-chain’ lipids. Many naturally occurring sphingolipids in mammalian cells are highly asymmetric, with chain lengths ranging from 2 to 28 carbons [9–11]. Recent studies have shown that some yeast strains also produce highly asymmetric glycerophospholipids with saturated tails that differ in length by up to 6 or 8 carbons [12,13]. It is increasingly clear that such

chain-asymmetric lipids are important for regulating biomembrane properties; however, we are only starting to understand their effects.

Previous studies of phospholipid membranes suggest there are primarily two ways the large differences in tail lengths are accommodated in the membrane. The longer of the tails either penetrate into the opposing leaflet to form interdigitated structures [14–16] or fold back onto themselves into the host leaflet [17–19]. Literature suggests both mechanisms are at play in chain-asymmetric lipid bilayers, and while these lipids form partially interdigitated bilayers in the fluid phase, the longer acyl tails remain highly dynamic and rapidly sample both their own and the opposing leaflet [19–25].

Both means of accommodating the chain length mismatch could significantly impact the membrane dynamics and elastic properties, but would likely have opposite effects. Simulations by den Otter and Shkulipa showed that the increased interdigitation in membranes composed of asymmetric lipids increased the friction (b) between the two bilayer leaflets [26]. The magnitude of b dictates both the energy required for the two bilayer leaflets to slide past one another as well as the timescales of these motion, and increasing b should slow down dynamic processes ranging from membrane fluctuations to rapid changes in cell shape [27–30]. On the other hand, the rapid movements of the longer acyl chain as it moves between the bilayer midplane and its host leaflet would lead to the formation of transient voids in the membrane that could influence the membrane elastic properties. To this end, recent simulation results by Frewein et al. suggested that the backbone tails and associated packing defects near the lipid backbone significantly impacted the lateral pressure profile of the bilayer, which in turn could have a larger effect on the membrane elastic properties and associated dynamic processes [19]. Moreover, both experimental and computational studies suggest that chain-asymmetric membranes are more compressible than analogous chain-symmetric lipid membranes [23–25]. This increased compressibility as well as the suggested formation of transient defects in chain-asymmetric lipid membranes should enhance the bending fluctuation dynamics.

Here we study the nanoscale bending dynamics in mixed-chain lipid membranes in the biologically relevant fluid phase using neutron spin echo spectroscopy (NSE). Because NSE is a time domain measurement, it is uniquely suited to measuring the membrane dynamics on the nanometer length scale and nanosecond time scale that can be affected by changes in interleaflet interactions, such as the friction between leaflets, as well as the presence of packing defects and changes in the membrane elasticity. We measure the bending dynamics of bilayers prepared with 1-myristoyl-2-stearoyl-sn-glycerol-3-phosphocholine (14:0-18:0 PC, MSPC) and 1-stearoyl-2-myristoyl-sn-glycero-3-phosphocholine (18:0-14:0 PC, SMPC), whose tails differ in length by 4 carbons, and compare the dynamics with those measured for a chain-symmetric lipid with the same average number of carbons in the acyl tail, 1,2-dipalmitoyl-sn-glycerco-3-phosphophocholine (di 16:0 PC, DPPC). We chose these model lipids as recent studies by Frewein et al. showed that these chain-asymmetric and analogous chain-symmetric lipids formed membranes with almost identical thicknesses and areas per lipids at the same temperature [19], allowing us to compare the effects of the chain length mismatch and degree of leaflet interdigitation on the nanoscale membrane dynamics with minimal competing effects from differences in d_B and A_L that are also known to impact the properties of interest. Moreover, these experiments allow us to compare the effects of not only the difference in chain lengths, but also how the tails are connected to the hydrophilic headgroup, on the dynamics of model chain-asymmetric lipid membranes.

2. Materials and Methods

2.1. Materials

Lipids, including 1,2-dipalmitoyl-sn-glycerco-3-phosphophochloine (di 16:0 PC, DPPC), 1-myristoyl-2-stearoyl-sn-glycerol-3-phosphocholine (14:0-18:0 PC, MSPC) and 1-stearoyl-2-myristoyl-sn-glycero-3-phosphocholine (18:0-14:0 PC, SMPC) were purchased from Avanti Polar Lipids as powders and used as received. Deuterium oxide (99.9% D) was purchased from Cambridge Isotopes.

2.2. Vesicle Preparation

Unilamellar vesicle solutions were prepared by extrusion through polycarbonate filters with a nominal pore diameter of 50 nm following well established procedures [31]. The final solution contained 50 mg of lipid per mL of D₂O, corresponding to a vesicle volume fraction (ϕ_V) ranging from ≈ 0.15 to 0.17. Samples measured at IN15 were extruded using a 100 nm filter and diluted to a concentration (c_{lipid}) of 20 mg/mL. Small angle neutron scattering (SANS) data were collected to ensure that the vesicles were predominately unilamellar (>95%) and there was not a significant population of paucilamellar vesicles that could affect the interpretation of the dynamics results. A summary of the vesicles sizes and volume fractions is given in Table 1.

Table 1. Summary of sample properties.

Sample	T_m (°C)	c_{lipid} (mg/mL)	R_H (nm)	ϕ_V
MSPC	40	20	54	0.089
		50	39	0.15
SMPC	30	20	58	0.095
		50	44	0.17
DPPC	41	50	36	0.15

2.3. Small Angle Neutron Scattering (SANS)

SANS data were collected on the NG3 vSANS instrument at the National Institute of Standards and Technology (NIST) Center for Neutron Research (NCNR) [32]. Data were collected over a combined q range of $0.01 \text{ nm}^{-1} < q < 4 \text{ nm}^{-1}$, where q is the magnitude of the scattering vector and is defined as $q = 4\pi/\lambda \sin(\theta/2)$ with scattering angle, θ , using neutron wavelengths (λ) of 0.6 nm or 1.1 nm with a wavelength distribution ($\Delta\lambda/\lambda$) of 0.12. The front and middle detector carriages were positioned at 1 m and 5 m or 4.5 m and 18.5 m, for the 0.6 nm and 1.1 nm wavelength configurations, respectively. SANS data were reduced using the macros provided by NIST [33] and analysed with a vesicle form factor that includes potential contributions from a small population of paucilamellar vesicles [31].

2.4. Dynamic Light Scattering (DLS)

Dynamic light scattering (DLS) measurements were performed with a Wyatt NanoStar Pro to determine the vesicle diffusion coefficient at infinite dilution (D_0). The samples were diluted 100× with D₂O to a concentration of 0.5 mg/mL corresponding to $\phi_V \approx 0.02$. DLS data were collected at 45 °C, and the samples were equilibrated at the measurement temperature for at least 15 min before the data were collected. The resulting D_0 values were used in the NSE data analysis as well as to calculate the hydrodynamic radius (R_H) of the vesicles according to the Stokes-Einstein equation, $R_H = \frac{k_B T}{6\pi\eta D_0}$, where η is the solvent viscosity.

2.5. Neutron Spin Echo Spectroscopy (NSE)

NSE measurements were performed on the NGA NSE Instrument at the NCNR with λ of 0.8 nm or 1.1 nm and $\Delta\lambda/\lambda \approx 0.2$ to access a q -values ranging from $0.4 \text{ nm}^{-1} < q < 1.1 \text{ nm}^{-1}$ and Fourier times (t) ranging from 0.01 ns to 100 ns [34]. The temperature was controlled within 0.5 °C using a recirculating bath. Samples were equilibrated at the desired temperatures for 30 min before the data collection. Data were corrected for the instrument resolution and the dynamic contributions from the D₂O solvent to give the normalized intermediate scattering function ($I(q, t)/I(q, 0)$) using the DAVE software package [35]. Additional NSE measurements were carried out on the IN15 spin-echo spectrometer at Institut Laue-Langevin (ILL), Grenoble, France [36]. Intermediate scattering functions were measured in the range of scattering vectors $q = 0.2 \text{ nm}^{-1}$ to 1.11 nm^{-1} using incoming neutron wavelengths of 0.8 nm, 1.0 nm and 1.2 nm. The accessed Fourier

time range was 0.01 ns to 300 ns. Samples were kept in quartz-cells of 1 mm pathlength and heated to 50 °C using a bath circulator.

3. Results

NSE is a quasielastic scattering technique that measures relaxation dynamics at nanometer length scales over time scales from picosecond to hundreds of nanoseconds and has been used to study collective dynamics on the length scale of the membrane itself in a number of model systems [37–40]. The measured intermediate scattering functions ($I(q, t)/I(q, 0)$) for MSPC (14:0-18:0 PC), SMPC (18:0-14:0 PC) and DPPC (16:0-16:0 PC) at the same temperature relative to their melting temperature, $T - T_m = 10$ °C, are shown in Figure 1 for a range of scattering vector (q) values from $0.37 \text{ nm}^{-1} < q < 1.3 \text{ nm}^{-1}$. These q -values correspond to length scales of $\approx 17 \text{ nm}$ to 5 nm .

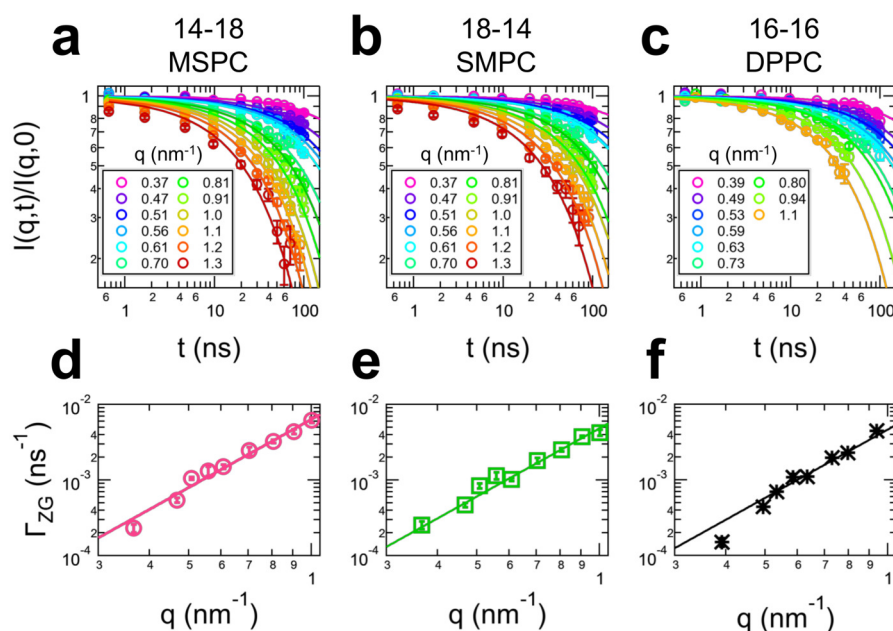


Figure 1. NSE data measured for tail-asymmetric lipid vesicles $\approx 80 \text{ nm}$ in diameter measured on the NGA-NSE at approximately the same relative temperature. Intermediate scattering functions measured for (a) MSPC, (b) SMPC, and (c) DPPC (points) and fits to Equation (1) (lines). Numbers in the legends of plots (a–c) indicate values of q with units of nm^{-1} . Corresponding relaxation rates (Γ_{ZG}) versus q for (d) MSPC, (e) SMPC and (f) DPPC (points) with fits to Equation (3) (lines). Experiments were performed at $T - T_m \approx 10$ °C. Error bars represent one standard deviation and in some cases are smaller than the symbols.

The solid lines are fits to the data considering the contributions from both the vesicle diffusion and membrane fluctuations that have been shown to contribute to the dynamics measured at the length scales and time scales accessible with NSE [37,41–43]

$$I(q, t)/I(q, 0) = \exp(-D_s q^2 t) \exp(-(\Gamma_{ZG} t)^{2/3}) \quad (1)$$

where the first term accounts for the self diffusion of the vesicles with diffusion coefficient D_s that takes into account the hydrodynamic interactions between vesicles at relatively high volume fractions [30,44] and the second term describes the membrane bending fluctuations following the Zilman-Granek formalism with relaxation rate Γ_{ZG} [41,45].

Values for D_s were calculated based on the diffusion coefficient at infinite dilution (D_0) determined from independent DLS measurements on diluted samples and the volume fraction of vesicles (ϕ_V) in the NSE sample calculated based on the known lipid masses and volumes and the hydrodynamic radii (R_H) of the vesicles that are reported in Table 1,

$$\frac{D_s}{D_0} = 1 - 1.832\phi_V - 0.219\phi_V^2 + \mathcal{O}(\phi_V^3). \quad (2)$$

Equation (2) was originally developed to describe diffusion in concentrated hard sphere solutions and has been shown to be accurate for hard sphere volume fractions ≤ 0.3 and work well for relatively concentrated lipid vesicle solutions such as those studied here [30,46,47].

The neutron scattering length density contrast between the lipid membranes and deuterated solvent used here made the NSE measurements most sensitive to the membrane height fluctuations dynamics that are also referred to as bending fluctuations. These dynamics were fit assuming that the measured relaxation rate is determined by a balance of the effective membrane rigidity ($\tilde{\kappa}$) and viscosity of the surrounding solvent, (η) [41,42,45,48].

$$\Gamma_{ZG} = 0.025 \frac{k_B T}{\eta} \sqrt{\frac{k_B T}{\tilde{\kappa}}} q^3 \quad (3)$$

It is important to note that the effective rigidity, $\tilde{\kappa}$, in Equation (3) is different from the bending modulus (κ) extracted from techniques like diffuse X-ray scattering or flicker spectroscopy that measure the equal-time average amplitude of the membrane height fluctuations. $\tilde{\kappa}$ includes effects from dissipation within the bilayer that need to be considered in the time domain, i.e., measurements of the membrane fluctuation relaxation dynamics [27,37,48,49].

As seen in Figure 1, the data were well fit with Equation (1) for $q < 1 \text{ nm}^{-1}$. The corresponding values of Γ_{ZG} also scaled with q^3 as predicted by Equation (3). These trends suggest that the dynamics measured for the tail-asymmetric lipid membranes at lower q -values were following the scaling seen in vesicles composed of chain-symmetric lipids [5,30,50] as well as compositionally asymmetric bilayers [51] reported in literature.

The data at the highest q values, $q > 1.0 \text{ nm}^{-1}$, that correspond to the length scales of $\approx 5 \text{ nm}$ deviated from the predicted scaling at short time scales, $t \leq 20 \text{ ns}$. The measured $I(q, t)/I(q, 0)$ did not approach 1 at short time scales, suggesting that faster dynamic processes were contributing to the NSE data and were not captured by the current analysis.

The values for $\tilde{\kappa}$ extracted from the NSE data for the chain-asymmetric lipids are compared with the results for a chain-symmetric lipid containing the same average number of CH_2 groups, DPPC, in Figure 2. The $\tilde{\kappa}$ values for MSPC and SMPC were similar and notably less than the value for DPPC. The $\approx 30\%$ to 40% reduction in $\tilde{\kappa}$ values highlights that the nanoscale dynamics were enhanced in chain-asymmetric lipid membranes.

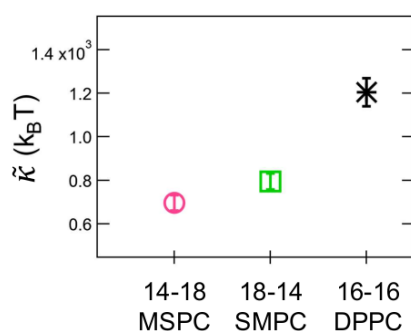


Figure 2. Comparison of $\tilde{\kappa}$ values for asymmetric and symmetric lipids with the same average number of carbons in the tails at the same relative temperature, $T - T_m \approx 10 \text{ }^\circ\text{C}$. Error bars represent the 95% confidence intervals on best fit value of $\tilde{\kappa}$ from plots Γ_{ZG} vs. q^3 using Equation (3).

Figure 3 compares $\tilde{\kappa}$ values determined from two separate NSE experiments performed on MSPC and SMPC vesicles that were prepared by extrusion through either 50 nm or 100 nm filters. The $\approx 100 \text{ nm}$ vesicles also contained a small amount of charged lipid to ensure they were unilamellar. The vesicle sizes and lipid concentrations used for the NSE

experiments are summarized in Table 1. The data from both SMPC samples were in good agreement and showed that $\tilde{\kappa}$ decreased with increasing temperature. It is not clear why there was a greater discrepancy in the $\tilde{\kappa}$ values for the different MSPC samples. The added charge and larger size of the vesicles extruded through the 100 nm filters (Table 1) would be expected to stiffen the membrane [52–54] or result in apparently slower dynamics [43,55], the opposite of the experimentally observed trends. The NSE data also suggested that the bending dynamics of the MSPC samples had a different temperature dependence than the SMPC samples. Estimates for the temperature dependence of $\tilde{\kappa}$ as $\alpha_{\tilde{\kappa}} = \tilde{\kappa}^{-1}(d\tilde{\kappa}/dT)$ gave $\alpha_{\tilde{\kappa}} \approx -0.02 \pm 0.001$ for SMPC at $T_m + 10$ °C and $\alpha_{\tilde{\kappa}} \approx 0$ for MSPC.

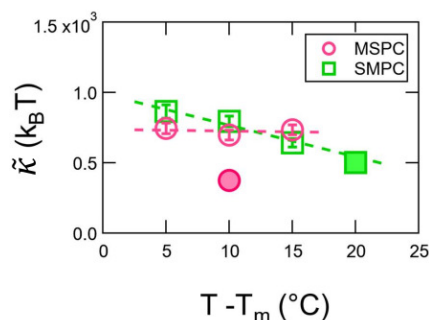


Figure 3. Temperature dependence of $\tilde{\kappa}$ measured for MSPC and SMPC lipid membranes. The dashed lines are linear fits to the data. Open symbols correspond to data for vesicles extruded through 50 nm filters measured on the NGA-NSE at the NCNR. Closed symbols correspond to vesicles extruded through 100 nm filters measured on the IN15 NSE at the ILL. Additional sample information is provided in Table 1. Error bars represent the 95% confidence intervals on best fit value of $\tilde{\kappa}$ and in some cases are smaller than the symbols.

4. Discussion

The NSE data show that membrane bending dynamics are enhanced in chain-asymmetric lipid bilayers compared to bilayers containing a chain-symmetric lipid with the same average number of carbons in the tails in the studied range of length scales and time scales. While these faster dynamics are seemingly counterintuitive to what is expected based on structural studies that show chain-asymmetric lipids form more interdigitated bilayers, even in the fluid phase, the results offer some evidence as to why yeast have been shown to compensate for a lack of unsaturated fatty acids by synthesizing saturated chain-asymmetric lipids [13,56]. It is well known that unsaturated chains, such as oleates, are more dynamic than their saturated counterparts and form softer membranes at a given temperature [57,58]. The present NSE data suggest that chain-asymmetric lipids also increase the membrane dynamics, indicating that the dynamics at the studied time scales are not significantly affected by the increased interdigitation [14,16,19] and computationally-predicted increase in friction between the leaflets [26].

An intriguing difference between tail unsaturation and asymmetry in length is their effects on the melting transition temperature of the lipids. The melting transition of unsaturated lipids typically occurs well below the freezing point of water ($T_m \ll 0$ °C) [59]. As such, physiological temperature corresponds to a relative temperature ($T - T_m$) on the order of 40 °C or more. Because the membrane dynamics increase with temperature above T_m , it is not surprising that an unsaturated lipid membrane is much more flexible at a given temperature than an analogous saturated lipid membrane with a much higher T_m . However, work by Nanda et al. showed that when the lipid dynamics were compared at the same relative temperature, the atoms in a saturated DMPC membrane were more mobile than in an unsaturated DOPC membrane [60]. Chain length asymmetry is also known to decrease T_m [61], yet the effects are not nearly as pronounced as unsaturation, and the results in Figure 2 clearly show that the chain asymmetric lipid membranes are more dynamic than the analogous symmetric lipid at the same $T - T_m$. This thought-provoking difference

perhaps suggests that chain length asymmetry is important for tuning membrane properties without significantly altering the phase transition temperatures in biomembranes.

A more quantitative comparison suggests that the $\approx 40\%$ decrease in $\tilde{\kappa}$ seen in the NSE data is consistent with previously reported decreases in the compressibility modulus of chain-asymmetric lipid membranes. As shown in Equation (3), the relaxation rate measured in NSE is determined by a balance of the viscosity of the surrounding solvent and the effective membrane rigidity, $\tilde{\kappa} = \kappa + 2h^2k_m$, where κ is the bending modulus as defined by the traditional Helfrich framework [62], h is the height of the neutral surface of the bilayer, and k_m is the monolayer compressibility modulus. The effective rigidity was first defined in work by Seifert and Langer, where the second term in the $\tilde{\kappa}$ expression accounts for the dissipation within the bilayer as the lipids need to rearrange to accommodate the local lipid density change at short length scales and fast time scales, such as those measured with NSE [27]. While the expression for $\tilde{\kappa}$ describes dynamic processes in the membrane, it can be rewritten in terms of the bilayer compressibility using well established relationships for the monolayer (k_m) and bilayer (K_A) compressibility moduli, $K_A = 2k_m$, and κ and K_A , $\kappa = \beta d_t^2 K_A$ [3], such that $\tilde{\kappa} = [h^2 + \beta d_t^2] K_A$. Here, β is a constant that describes the degree of coupling between the bilayer leaflets ranging from 1/12 for completely coupled leaflets to 1/48 for completely uncoupled leaflets and d_t is the thickness of the hydrophobic region of the bilayer.

The measured 30% to 40% reduction in $\tilde{\kappa}$ suggests a comparable decrease in K_A term and is in good agreement with previous results that have shown mixed-chain lipid membranes are more compressible than comparable symmetric lipids. Ali et al. previously showed that the in-plane compressibility modulus of chain-asymmetric lipid monolayers at the air-water interface was $\approx 20\%$ to 25% lower than corresponding chain-symmetric lipid [23]. Similarly, Illya et al. also reproduced this finding in dissipative particle dynamics simulations, where changing the chains from symmetric to asymmetric with the same total number of beads reduced the compressibility modulus of the bilayer by up to 40% [24]. However, it is important to note that it is currently unknown if and how the chain-length asymmetry affects the values of h and/or β compared to values known for chain symmetric lipid membranes. Future experimental and computational studies of κ , K_A , h , and by extension, β , will provide further insights into how chain length asymmetry not only affects the mechanical properties of the bilayers, but also how stresses are transferred between the leaflets.

In addition to the bending mode discussed above, Seifert and Langer predict that there is also a second, slower mode due to the slipping of the two leaflets past each other that contributes to the membrane height fluctuations at short length scales, and the relaxation rate of the slow slipping mode is related to the interleaflet friction, b [27]. Monroy and colleagues also reported evidence of two relaxation modes in NSE data for some lipid systems, where the relaxation rate of what they called the hybrid, slipping mode was related to b [63,64]. While we did not see evidence of a slow slipping mode in the present NSE data, it would be highly interesting to extend studies of the asymmetric lipid membrane dynamics to even longer time scales using techniques like dynamic light scattering [65], dynamic optical displacement spectroscopy [66], or x-ray photon correlation spectroscopy [67] that are sensitive to the membrane dynamics on the microsecond time scale. Given that b has been shown to increase in mixed-chain lipid membranes [26], it is likely that chain length asymmetry will have different effects on the membrane dynamics at the microsecond timescales than at the nanosecond time scales studied here.

While the NSE data at long times were well described by a single stretched exponential for bending fluctuations (Equation (3)), the data at high q and short times ($t < 20$ ns) deviated from the predicted scaling. As seen in Figure 1, the measured $I(q, t)/I(q, 0) \neq 1$ as $t \rightarrow 0$ which may suggest the presence of a faster dynamic process not described by the model used to fit the data. Previous work by Gupta and colleagues noted similar deviations in NSE data for some lipid systems [50,68] that have been attributed to confined motions of the lipid acyl tails [50,68] or potential peristaltic thickness fluctuations or so

called Brochard–Lennon “red blood cell” modes [69]. We also emphasize that NSE data interpretation and background subtraction become more challenging at these high q values, as shown by Hoffman [43], where the coherent and incoherent scattering signals are comparable in magnitude. As such, this work can not distinguish between the potential reasons for the discrepancy between the measured data and well-established models for the collective bending fluctuations at high q and short t , but does suggest that further studies of the coherent and incoherent dynamics in mixed-chain lipid membranes are not only needed, but will be highly interesting.

Quite surprisingly, the present NSE data, as well as previous results in the literature, suggest that chain-length asymmetry can soften the membrane but does not significantly alter the overall membrane thickness or area per lipid [19]. Direct links between the structure and elastic and viscous properties of membranes have been established for chain-symmetric lipids where faster dynamics and lower κ values are usually reported for more disordered and thinner bilayers [3,70–72]. We recently showed that mixing symmetric di 14:0 PC (DMPC) and di 18:0 PC (DSPC) lipids with a 4 carbon mismatch in tail lengths enhanced the dynamics compared to either of the pure component membranes, similar to the results seen for the chain-asymmetric lipids studied here where a 14:0 and 18:0 chain are attached to the same headgroup [72]. However, the enhanced dynamics in the binary mixtures of symmetric lipids were directly related to changes in the area per lipid (A_L), where κ , the compressibility modulus, and membrane viscosity collapsed on to respective scaling plots with A_L . The structures of MSPC, SMPC, and DPPC have been reported to vary by less than 1% at the same temperature [19], yet here we see that the membrane dynamics and effective rigidity vary by upwards of 40%. Likewise, the 40% change in the compressibility modulus reported by Illya et al. for chain-asymmetric lipid membranes was associated with a less than 1% change in the bilayer thickness [24]. Schram and Thompson also reported unusual disparity between the diffusion coefficient of chain-asymmetric lipids (D) and changes in lipid packing and/or A_L and suggested that increased dynamics of the longer acyl tail compensated for any difference (or lack thereof) in the molecular packing and A_L [22].

The lack of temperature dependence seen in $\tilde{\kappa}$ for MSPC was also unexpected. The bending rigidity and area compressibility modulus of several symmetric lipid membranes have been shown to modestly decrease with increasing temperature well above T_m [5,73,74]. The value of $\alpha_{\tilde{\kappa}} \approx -0.020 \pm 0.001$ for SMPC was also in good agreement with values estimated from previous NSE studies of chain-symmetric bilayers with 14 carbon (DMPC) and 18 carbon (DSPC) tails that were ≈ -0.015 and -0.018 , respectively, [5]. These changes in the membrane dynamics and associated elastic properties are related to the increased *trans-gauche* isomerization of the lipid acyl tails with increasing temperature [74], perhaps suggesting that the changes in the MSPC lipid tail dynamics with temperature are less pronounced than typically seen in chain-symmetric lipid bilayers. This speculation for the observed trends in MSPC is consistent by previous NMR studies that suggested changes in the order parameter (S_{CD}) with temperature were less pronounced in chain-asymmetric lipid bilayers than typically seen in chain-symmetric lipids bilayers [20].

The striking difference in temperature trends of MSPC and SMPC could be also due to the configuration of the glycerol-backbone of the lipids. Recent SAXS/SANS experiments and simulations [19] showed that SMPC has a higher degree of chain interdigitation than MSPC at 50 °C, suggesting that its sn-1 position is located closer to the bilayer center than sn-2. If the glycerol configuration changes with temperature, this has necessarily opposite effects on interdigitation for these lipids, as for SMPC the longer stearyl-chain is attached at the sn-1 position, while for MSPC at sn-2. If an increase in temperature further pushes the sn-1 chain towards the bilayer center, the difference in effective chain length of MSPC decreases, making the membrane more rigid. This effect is countered by a temperature-induced softening due to bilayer thinning and increase in hydrocarbon chain disorder. On the contrary, chain length asymmetry in SMPC would be increased by this effect, and therefore, SMPC behaves in a similar way as a chain-symmetric lipid. Further

SAXS measurements could give insight into the temperature trend of interdigitation, and therefore, the corresponding glycerol-configuration of these lipids.

5. Conclusions

Here we studied the nanoscale bending fluctuations in mixed-chain lipid membranes using NSE. Quite interestingly, the chain-asymmetric lipid bilayers were more dynamic than an analogous chain symmetric lipid bilayer with the same average number of carbons in the tail despite reports of chain-asymmetric lipid bilayers being more interdigitated. These results add to the evidence that the interdigitation in fluid mixed-chain lipid membranes is highly dynamic and suggest that the effects of previously reported rapid motions of the longer acyl tails propagate to the collective membrane motions involving tens to hundreds of lipids on the nanosecond time scales. Future studies aimed at understanding how the degree of asymmetry affects dynamic processes ranging from the acyl tail motions to the collective bending and thickness fluctuations will further bridge the molecular and macroscopic scales and may help further reveal the biological importance of this unusual class of lipids.

Author Contributions: Conceptualization, E.G.K., M.P.K.F. and M.N.; methodology, E.G.K., M.P.K.F., O.C. and M.N.; formal analysis, E.G.K., M.P.K.F., O.C. and M.N.; investigation, E.G.K., M.P.K.F. and M.N.; writing—original draft preparation, E.G.K., M.P.K.F. and M.N. All authors have read and agreed to the published version of the manuscript.

Funding: Access to the NGA-NSE and vSANS instruments was provided by the Center for High Resolution Neutron Scattering, a partnership between the National Institute of Standards and Technology and the National Science Foundation under DMR-2010792. Certain equipment, instruments or materials are identified in this paper to adequately specify the experimental details. Such identification does not imply recommendation by the National Institute of Standards and Technology nor does it imply that the materials are necessarily the best available for the purpose. This research was also supported by the ILL graduate school, Ph.D. No. 181-19.

Data Availability Statement: SANS, DLS and NGA-NSE data used in writing this manuscript are available from the NIST public data repository at <https://doi.org/10.18434/mds2-2829> IN15 NSE data are available from the ILL data repository at <https://doi.org/10.5291/ILL-DATA.9-13-953>.

Conflicts of Interest: The authors declare no conflict of interest.

Abbreviations

The following abbreviations are used in this manuscript:

DLS	Dynamic Light Scattering
DMPC	1,2-dimyristoyl-sn-glycerco-3-phosphocholine (di 14:0 PC)
DOPC	1,2-dioleoyl-sn-glycerco-3-phosphocholine (di 18:1 PC)
DPPC	1,2-dipalmitoyl-sn-glycerco-3-phosphocholine (di 16:0 PC)
DSPC	1,2-distearoyl-sn-glycerco-3-phosphocholine (di 18:0 PC)
MSPC	1-myristoyl-2-stearoyl-sn-glycerol-3-phosphocholine (14:0-18:0 PC)
NSE	Neutron Spin Echo Spectroscopy
SANS	Small Angle Neutron Scattering
SAXS	Small Angle X-ray Scattering
SMPC	1-stearoyl-2-myristoyl-sn-glycerco-3-phosphocholine (18:0-14:0 PC)

References

1. Kučerka, N.; Nieh, M.P.; Katsaras, J. Fluid phase lipid areas and bilayer thicknesses of commonly used phosphatidylcholines as a function of temperature. *Biochim. Biophys. Acta (BBA)-Biomembr.* **2011**, *1808*, 2761–2771. [[CrossRef](#)] [[PubMed](#)]
2. Kučerka, N.; Heberle, F.A.; Pan, J.; Katsaras, J. Structural significance of lipid diversity as studied by small angle neutron and X-ray scattering. *Membranes* **2015**, *5*, 454–472. [[CrossRef](#)] [[PubMed](#)]
3. Rawicz, W.; Olbrich, K.C.; McIntosh, T.; Needham, D.; Evans, E. Effect of chain length and unsaturation on elasticity of lipid bilayers. *Biophys. J.* **2000**, *79*, 328–339. [[CrossRef](#)] [[PubMed](#)]

4. Woodka, A.C.; Butler, P.D.; Porcar, L.; Farago, B.; Nagao, M. Lipid bilayers and membrane dynamics: Insight into thickness fluctuations. *Phys. Rev. Lett.* **2012**, *109*, 058102. [[CrossRef](#)] [[PubMed](#)]
5. Nagao, M.; Kelley, E.G.; Ashkar, R.; Bradbury, R.; Butler, P.D. Probing elastic and viscous properties of phospholipid bilayers using neutron spin echo spectroscopy. *J. Phys. Chem. Lett.* **2017**, *8*, 4679–4684. [[CrossRef](#)] [[PubMed](#)]
6. Faizi, H.A.; Dimova, R.; Vlahovska, P.M. A vesicle microrheometer for high-throughput viscosity measurements of lipid and polymer membranes. *Biophys. J.* **2022**, *121*, 910–918. [[CrossRef](#)]
7. Nagle, J.F.; Tristram-Nagle, S. Structure of lipid bilayers. *Biochim. Biophys. Acta (BBA)-Rev. Biomembr.* **2000**, *1469*, 159–195. [[CrossRef](#)]
8. Lorent, J.; Levental, K.; Ganesan, L.; Rivera-Longsworth, G.; Sezgin, E.; Doktorova, M.; Lyman, E.; Levental, I. Plasma membranes are asymmetric in lipid unsaturation, packing and protein shape. *Nat. Chem. Biol.* **2020**, *16*, 644–652. [[CrossRef](#)]
9. Goñi, F.M.; Alonso, A. Biophysics of sphingolipids I. Membrane properties of sphingosine, ceramides and other simple sphingolipids. *Biochim. Biophys. Acta (BBA)-Biomembr.* **2006**, *1758*, 1902–1921. [[CrossRef](#)]
10. Jimenez-Rojo, N.; Garcia-Arribas, A.B.; Sot, J.; Alonso, A.; Goni, F.M. Lipid bilayers containing sphingomyelins and ceramides of varying N-acyl lengths: A glimpse into sphingolipid complexity. *Biochim. Biophys. Acta (BBA)-Biomembr.* **2014**, *1838*, 456–464. [[CrossRef](#)]
11. Fujimoto, T.; Parmryd, I. Interleaflet coupling, pinning, and leaflet asymmetry—Major players in plasma membrane nanodomain formation. *Front. Cell Dev. Biol.* **2017**, *4*, 155. [[CrossRef](#)] [[PubMed](#)]
12. Makarova, M.; Peter, M.; Balogh, G.; Glatz, A.; MacRae, J.L.; Mora, N.L.; Booth, P.; Makeyev, E.; Vigh, L.; Oliferenko, S. Delineating the rules for structural adaptation of membrane-associated proteins to evolutionary changes in membrane lipidome. *Curr. Biol.* **2020**, *30*, 367–380. [[CrossRef](#)] [[PubMed](#)]
13. Reinhard, J.; Mattes, C.; Vãth, K.; Radanović, T.; Surma, M.A.; Klose, C.; Ernst, R. A quantitative analysis of cellular lipid compositions during acute proteotoxic ER stress reveals specificity in the production of asymmetric lipids. *Front. Cell Dev. Biol.* **2020**, *8*, 756. [[CrossRef](#)] [[PubMed](#)]
14. Huang, C.; Mason, J.; Levin, I. Raman spectroscopic study of saturated mixed-chain phosphatidylcholine multilamellar dispersions. *Biochemistry* **1983**, *22*, 2775–2780. [[CrossRef](#)]
15. McIntosh, T.; Simon, S.; Ellington Jr, J.; Porter, N. New structural model for mixed-chain phosphatidylcholine bilayers. *Biochemistry* **1984**, *23*, 4038–4044. [[CrossRef](#)]
16. Hui, S.; Mason, J.; Huang, C. Acyl chain interdigitation in saturated mixed-chain phosphatidylcholine bilayer dispersions. *Biochemistry* **1984**, *23*, 5570–5577. [[CrossRef](#)] [[PubMed](#)]
17. Halladay, H.N.; Stark, R.E.; Ali, S.; Bittman, R. Magic-angle spinning NMR studies of molecular organization in multibilayers formed by 1-octadecanoyl-2-decanoyl-sn-glycero-3-phosphocholine. *Biophys. J.* **1990**, *58*, 1449–1461. [[CrossRef](#)]
18. Zhu, T.; Caffrey, M. Thermodynamic, thermomechanical, and structural properties of a hydrated asymmetric phosphatidylcholine. *Biophys. J.* **1993**, *65*, 939–954. [[CrossRef](#)]
19. Frewein, M.P.; Doktorova, M.; Heberle, F.A.; Scott, H.L.; Semeraro, E.F.; Porcar, L.; Pabst, G. Structure and interdigitation of chain-asymmetric phosphatidylcholines and milk sphingomyelin in the fluid phase. *Symmetry* **2021**, *13*, 1441. [[CrossRef](#)]
20. Lewis, R.; McElhaney, R.N.; Monck, M.A.; Cullis, P.R. Studies of highly asymmetric mixed-chain diacyl phosphatidylcholines that form mixed-interdigitated gel phases: Fourier transform infrared and 2H NMR spectroscopic studies of hydrocarbon chain conformation and orientational order in the liquid-crystalline state. *Biophys. J.* **1994**, *67*, 197–207.
21. Mason, J.T. Properties of phosphatidylcholine bilayers as revealed by mixed-acyl phospholipid fluorescent probes containing n-(9-anthroyloxy) fatty acids. *Biochim. Biophys. Acta (BBA)-Biomembr.* **1994**, *1194*, 99–108. [[CrossRef](#)]
22. Schram, V.; Thompson, T.E. Interdigitation does not affect translational diffusion of lipids in liquid crystalline bilayers. *Biophys. J.* **1995**, *69*, 2517–2520. [[CrossRef](#)] [[PubMed](#)]
23. Ali, S.; Smaby, J.M.; Momsen, M.M.; Brockman, H.L.; Brown, R.E. Acyl chain-length asymmetry alters the interfacial elastic interactions of phosphatidylcholines. *Biophys. J.* **1998**, *74*, 338–348. [[CrossRef](#)]
24. Illya, G.; Lipowsky, R.; Shillcock, J. Effect of chain length and asymmetry on material properties of bilayer membranes. *J. Chem. Phys.* **2005**, *122*, 244901. [[CrossRef](#)] [[PubMed](#)]
25. Dan, N. Lipid tail chain asymmetry and the strength of membrane-induced interactions between membrane proteins. *Biochim. Biophys. Acta (BBA)-Biomembr.* **2007**, *1768*, 2393–2399. [[CrossRef](#)] [[PubMed](#)]
26. den Otter, W.K.; Shkulipa, S. Intermonolayer friction and surface shear viscosity of lipid bilayer membranes. *Biophys. J.* **2007**, *93*, 423–433. [[CrossRef](#)] [[PubMed](#)]
27. Seifert, U.; Langer, S.A. Viscous modes of fluid bilayer membranes. *EPL (Europhys. Lett.)* **1993**, *23*, 71. [[CrossRef](#)]
28. Shkulipa, S.; den Otter, W.K.; Briels, W.J. Thermal undulations of lipid bilayers relax by intermonolayer friction at submicrometer length scales. *Phys. Rev. Lett.* **2006**, *96*, 178302. [[CrossRef](#)]
29. Anthony, A.A.; Sahin, O.; Yapici, M.K.; Rogers, D.; Honerkamp-Smith, A.R. Systematic measurements of interleaflet friction in supported bilayers. *Biophys. J.* **2022**, *121*, 2981–2993. [[CrossRef](#)]
30. Kelley, E.G.; Blick, E.E.; Prabhu, V.M.; Butler, P.D.; Nagao, M. Interactions, Diffusion, and Membrane Fluctuations in Concentrated Unilamellar Lipid Vesicle Solutions. *Front. Phys.* **2022**, *10*, 866024. [[CrossRef](#)]
31. Scott, H.L.; Skinkle, A.; Kelley, E.G.; Waxham, M.N.; Levental, I.; Heberle, F.A. On the Mechanism of Bilayer Separation by Extrusion, or Why Your LUVs Are Not Really Unilamellar. *Biophys. J.* **2019**, *117*, 1381–1386. [[CrossRef](#)] [[PubMed](#)]

32. Barker, J.; Moyer, J.; Kline, S.; Jensen, G.; Cook, J.; Gagnon, C.; Kelley, E.; Chabot, J.P.; Maliszewskyj, N.; Parikh, C.; et al. The very small angle neutron scattering instrument at the National Institute of Standards and Technology. *J. Appl. Crystallogr.* **2022**, *55*, 271–283. [[CrossRef](#)] [[PubMed](#)]
33. Kline, S.R. Reduction and analysis of SANS and USANS data using IGOR Pro. *J. Appl. Crystallogr.* **2006**, *39*, 895–900. [[CrossRef](#)]
34. Rosov, N.; Rathgeber, S.; Monkenbusch, M. Neutron Spin Echo Spectroscopy at the NIST Center for Neutron Research; *ACS Symp. Ser.* **1999**, *739*, 103–116.
35. Azuah, R.T.; Kneller, L.R.; Qiu, Y.; Tregenna-Piggott, P.L.; Brown, C.M.; Copley, J.R.; Dimeo, R.M. DAVE: A comprehensive software suite for the reduction, visualization, and analysis of low energy neutron spectroscopic data. *J. Res. Natl. Inst. Stand. Technol.* **2009**, *114*, 341. [[CrossRef](#)]
36. Schleger, P.; Alefeld, B.; Barthelemy, J.; Ehlers, G.; Farago, B.; Giraud, P.; Hayes, C.; Kollmar, A.; Lartigue, C.; Mezei, F.; et al. The long-wavelength neutron spin-echo spectrometer IN15 at the Institut Laue-Langevin. *Phys. B Condens. Matter* **1997**, *241*, 164–165. [[CrossRef](#)]
37. Kelley, E.G.; Butler, P.D.; Nagao, M. 4. Collective dynamics in model biological membranes measured by neutron spin echo spectroscopy. In *Characterization of Biological Membranes*; de Gruyter: Berlin, Germany, 2019; pp. 131–176.
38. Gupta, S.; De Mel, J.U.; Schneider, G.J. Dynamics of liposomes in the fluid phase. *Curr. Opin. Colloid Interface Sci.* **2019**, *42*, 121–136. [[CrossRef](#)]
39. Kinnun, J.J.; Scott, H.L.; Ashkar, R.; Katsaras, J. Biomembrane Structure and Material Properties Studied With Neutron Scattering. *Front. Chem.* **2021**, *9*, 203. [[CrossRef](#)]
40. Gupta, S.; Ashkar, R. The dynamic face of lipid membranes. *Soft Matter* **2021**, *17*, 6910–6928. [[CrossRef](#)]
41. Zilman, A.; Granek, R. Undulations and dynamic structure factor of membranes. *Phys. Rev. Lett.* **1996**, *77*, 4788. [[CrossRef](#)]
42. Watson, M.C.; Peng, Y.; Zheng, Y.; Brown, F.L. The intermediate scattering function for lipid bilayer membranes: From nanometers to microns. *J. Chem. Phys.* **2011**, *135*, 194701. [[CrossRef](#)] [[PubMed](#)]
43. Hoffmann, I. Data Analysis and Background Subtraction in Neutron Spin Echo Spectroscopy. *Front. Phys.* **2021**, *8*, 602. [[CrossRef](#)]
44. Liu, Y. Intermediate scattering function for macromolecules in solutions probed by neutron spin echo. *Phys. Rev. E* **2017**, *95*, 020501. [[CrossRef](#)] [[PubMed](#)]
45. Zilman, A.G.; Granek, R. Membrane dynamics and structure factor. *Chem. Phys.* **2002**, *284*, 195–204. [[CrossRef](#)]
46. Gapinski, J.; Wilk, A.; Patkowski, A.; Häussler, W.; Banchio, A.; Pecora, R.; Nägele, G. Diffusion and microstructural properties of solutions of charged nanosized proteins: Experiment versus theory. *J. Chem. Phys.* **2005**, *123*, 054708. [[CrossRef](#)]
47. Banchio, A.J.; Nägele, G. Short-time transport properties in dense suspensions: From neutral to charge-stabilized colloidal spheres. *J. Chem. Phys.* **2008**, *128*, 104903.
48. Watson, M.C.; Brown, F.L. Interpreting membrane scattering experiments at the mesoscale: The contribution of dissipation within the bilayer. *Biophys. J.* **2010**, *98*, L9–L11. [[CrossRef](#)]
49. Nagle, J.F. Measuring the bending modulus of lipid bilayers with cholesterol. *Phys. Rev. E* **2021**, *104*, 044405. [[CrossRef](#)]
50. Gupta, S.; De Mel, J.U.; Perera, R.M.; Zolnierczuk, P.; Bleuel, M.; Faraone, A.; Schneider, G.J. Dynamics of Phospholipid Membranes beyond Thermal Undulations. *J. Phys. Chem. Lett.* **2018**, *9*, 2956–2960. [[CrossRef](#)]
51. Rickeard, B.W.; Nguyen, M.H.; DiPasquale, M.; Yip, C.G.; Baker, H.; Heberle, F.A.; Zuo, X.; Kelley, E.G.; Nagao, M.; Marquardt, D. Transverse lipid organization dictates bending fluctuations in model plasma membranes. *Nanoscale* **2020**, *12*, 1438–1447. [[CrossRef](#)]
52. Winterhalter, M.; Helfrich, W. Effect of surface charge on the curvature elasticity of membranes. *J. Phys. Chem.* **1988**, *92*, 6865–6867. [[CrossRef](#)]
53. Winterhalter, M.; Helfrich, W. Bending elasticity of electrically charged bilayers: Coupled monolayers, neutral surfaces, and balancing stresses. *J. Phys. Chem.* **1992**, *96*, 327–330. [[CrossRef](#)]
54. Dimova, R. Recent developments in the field of bending rigidity measurements on membranes. *Adv. Colloid Interface Sci.* **2014**, *208*, 225–234. [[CrossRef](#)] [[PubMed](#)]
55. Monkenbusch, M.; Holderer, O.; Frielinghaus, H.; Byelov, D.; Allgaier, J.; Richter, D. Bending moduli of microemulsions; comparison of results from small angle neutron scattering and neutron spin-echo spectroscopy. *J. Phys. Condens. Matter* **2005**, *17*, S2903. [[CrossRef](#)]
56. Meyer, F.; Bloch, K. Metabolism of stearolic acid in yeast. *J. Biol. Chem.* **1963**, *238*, 2654–2659. [[CrossRef](#)]
57. Ballweg, S.; Ernst, R. Control of membrane fluidity: The OLE pathway in focus. *Biol. Chem.* **2017**, *398*, 215–228. [[CrossRef](#)]
58. Budin, I.; de Rond, T.; Chen, Y.; Chan, L.J.G.; Petzold, C.J.; Keasling, J.D. Viscous control of cellular respiration by membrane lipid composition. *Science* **2018**, *362*, 1186–1189. [[CrossRef](#)]
59. Koynova, R.; Caffrey, M. Phases and phase transitions of the phosphatidylcholines. *Biochim. Biophys. Acta (BBA)-Rev. Biomembr.* **1998**, *1376*, 91–145. [[CrossRef](#)]
60. Nanda, H.; Sakai, V.G.; Khodadadi, S.; Tyagi, M.S.; Schwabach, E.J.; Curtis, J.E. Relaxation dynamics of saturated and unsaturated oriented lipid bilayers. *Soft Matter* **2018**, *14*, 6119–6127. [[CrossRef](#)]
61. Marsh, D. Analysis of the bilayer phase transition temperatures of phosphatidylcholines with mixed chains. *Biophys. J.* **1992**, *61*, 1036–1040. [[CrossRef](#)]
62. Helfrich, W. Steric interaction of fluid membranes in multilayer systems. *Z. Naturforschung A* **1978**, *33*, 305–315. [[CrossRef](#)]

63. Arriaga, L.; Rodriguez-Garcia, R.; López-Montero, I.; Farago, B.; Hellweg, T.; Monroy, F. Dissipative curvature fluctuations in bilayer vesicles: Coexistence of pure-bending and hybrid curvature-compression modes. *Eur. Phys. J. E* **2010**, *31*, 105–113. [[CrossRef](#)] [[PubMed](#)]
64. Mell, M.; Moleiro, L.H.; Hertle, Y.; López-Montero, I.; Cao, F.J.; Fouquet, P.; Hellweg, T.; Monroy, F. Fluctuation dynamics of bilayer vesicles with intermonolayer sliding: Experiment and theory. *Chem. Phys. Lipids* **2015**, *185*, 61–77. [[CrossRef](#)] [[PubMed](#)]
65. Hirn, R.; Bayerl, T.M.; Rädler, J.O.; Sackmann, E. Collective membrane motions of high and low amplitude, studied by dynamic light scattering and micro-interferometry. *Faraday Discuss.* **1999**, *111*, 17–30. [[CrossRef](#)] [[PubMed](#)]
66. Monzel, C.; Schmidt, D.; Kleusch, C.; Kirchenbühler, D.; Seifert, U.; Smith, A.; Sengupta, K.; Merkel, R. Measuring fast stochastic displacements of bio-membranes with dynamic optical displacement spectroscopy. *Nat. Commun.* **2015**, *6*, 8162. [[CrossRef](#)]
67. Falus, P.; Borthwick, M.; Mochrie, S. Fluctuation dynamics of block copolymer vesicles. *Phys. Rev. Lett.* **2005**, *94*, 016105. [[CrossRef](#)]
68. Gupta, S.; Schneider, G.J. Modeling the dynamics of phospholipids in the fluid phase of liposomes. *Soft Matter* **2020**, *16*, 3245–3256. [[CrossRef](#)]
69. Granek, R. Comment on “Dynamics of Phospholipid Membranes beyond Thermal Undulations”. *J. Phys. Chem. B* **2019**, *123*, 5665–5666. [[CrossRef](#)]
70. Nagle, J.F. Introductory lecture: Basic quantities in model biomembranes. *Faraday Discuss.* **2013**, *161*, 11–29. [[CrossRef](#)]
71. Doktorova, M.; Harries, D.; Khelashvili, G. Determination of bending rigidity and tilt modulus of lipid membranes from real-space fluctuation analysis of molecular dynamics simulations. *Phys. Chem. Chem. Phys.* **2017**, *19*, 16806–16818. [[CrossRef](#)]
72. Kelley, E.G.; Butler, P.D.; Ashkar, R.; Bradbury, R.; Nagao, M. Scaling relationships for the elastic moduli and viscosity of mixed lipid membranes. *Proc. Natl. Acad. Sci. USA* **2020**, *117*, 23365–23373. [[CrossRef](#)] [[PubMed](#)]
73. Meleard, P.; Gerbeaud, C.; Pott, T.; Fernandez-Puente, L.; Bivas, I.; Mitov, M.D.; Dufourcq, J.; Bothorel, P. Bending elasticities of model membranes: Influences of temperature and sterol content. *Biophys. J.* **1997**, *72*, 2616–2629. [[CrossRef](#)] [[PubMed](#)]
74. Pan, J.; Tristram-Nagle, S.; Kučerka, N.; Nagle, J.F. Temperature dependence of structure, bending rigidity, and bilayer interactions of dioleoylphosphatidylcholine bilayers. *Biophys. J.* **2008**, *94*, 117–124. [[CrossRef](#)] [[PubMed](#)]

Disclaimer/Publisher’s Note: The statements, opinions and data contained in all publications are solely those of the individual author(s) and contributor(s) and not of MDPI and/or the editor(s). MDPI and/or the editor(s) disclaim responsibility for any injury to people or property resulting from any ideas, methods, instructions or products referred to in the content.